Engineering Science & Technology
https://ojs.wiserpub.com/index.php/EST/

UNIVERSAL WISER PUBLISHER

Research Article

Simulation of Medium-Duty Truck Equipped with an Air-Assisted Hydraulic Hybrid Drive System

Kadir Aydin[*]

Department of Mechanical Engineering, Ostim Technical University, Ankara, Türkiye
E-mail: kadir.aydin@ostimteknik.edu.tr

Received: 29 May 2026; **Revised:** 30 June 2026; **Accepted:** 17 July 2026

Abstract: Heavy-duty commercial vehicles such as refuse trucks, urban delivery vans, transit buses and construction machinery are characterized by frequent stop-and-go duty cycles in which a significant share of the kinetic energy delivered by the prime mover is dissipated as heat at the friction brakes. The Hydraulic Hybrid Vehicle (HHV) architecture stores this otherwise-wasted braking energy in a hydro-pneumatic accumulator and releases it during the subsequent acceleration phase, exploiting the very high-power density of fluid-power components compared with electrochemical batteries. This paper presents an updated review of HHV powertrain architectures, including parallel, series and power-split configurations, together with the dynamic models of their principal sub-systems: the diesel engine, the bent-axis variable-displacement pump/motor, the hydro-pneumatic accumulator, the air tank with pressure exchanger, and the multi-stage reciprocating compressor. A forward-facing closed-loop simulation environment developed in MATLAB/Simulink is used to evaluate the theoretical and real-world energy-recovery efficiency of a Class VI medium-duty truck (gross mass 7,340 kg) equipped with an air-assisted series hydraulic hybrid drive over the Federal Urban Driving Schedule (FUDS). Theoretical recovery efficiencies of up to 0.89 and real (component-loss-corrected) values of up to 0.61 are obtained, with both metrics decreasing as the share of cruising relative to total cycle time increases. Recent peer-reviewed and demonstration data are reviewed: real-driving emissions tests reported in 2024 confirm fuel-consumption reductions of approximately 17% on urban routes, while Electro-Hydraulic Hybrid Vehicles (EHHV) configurations combining a battery, an electric machine and a hydraulic accumulator are emerging as a promising response to the European Union 2024/1257 (Euro VII) and 2024 CO_2 standards that mandate a 90% CO_2 reduction for new heavy-duty vehicles by 2040. The discussion concludes that hydraulic hybridization remains the most cost-effective and durable pathway for vocational duty cycles dominated by high-power, short-duration transients and that further work should focus on intelligent supervisory control, plug-in air/oil pre-charging, and integration of the accumulator with battery-electric and fuel-cell powertrains.

Keywords: hydraulic hybrid vehicle, regenerative braking, hydro-pneumatic accumulator, series hybrid, electro-hydraulic hybrid, heavy-duty truck, energy management strategy, fuel economy

1. Introduction

Road freight is the backbone of trade in Europe, where heavy goods vehicles transport approximately 77% of all overland freight while accounting for slightly more than one quarter of the greenhouse-gas emissions of the road

DOI: https://doi.org/10.37256/est.72202610228

transport sector and around 6% of the total European Union greenhouse-gas inventory [1]. The new Euro VII regulation, adopted as Regulation (EU) 2024/1257, harmonizes pollutant limits across light- and heavy-duty vehicles, tightens NO_x and CO ceilings, lowers the particle-number size limit from 23 nm to 10 nm, introduces gravimetric limits for N_2O and NH_3, and brings non-tailpipe particulate emissions from brakes and tires under regulatory control [2]. In parallel, the revised Regulation (EU) 2024/1610 establishes binding fleet-average CO_2 reduction targets of 45% from 2030, 65% from 2035 and 90% from 2040 relative to the 2019 baseline, and a 100% zero-emission requirement for new urban buses by 2035 [3]. These targets accelerate the search for propulsion concepts that combine the energy density of liquid fuels with the regenerative capability of an electrified driveline.

Hybrid-electric powertrains have so far attracted the most public attention, but in heavy-duty applications they suffer from two intrinsic disadvantages: the relatively low specific power of automotive lithium-ion batteries, which limits the rate at which braking energy can be captured during severe deceleration, and the limited cycle life of those batteries when subjected to the deep, frequent charge/discharge cycles typical of refuse, delivery and urban-bus duty cycles [4], [5]. The Hydraulic Hybrid Vehicle (HHV) addresses both limitations by storing kinetic energy in a hydro-pneumatic accumulator, in which a pre-charged inert gas is compressed by a hydraulic fluid driven by an axial-piston pump/motor coupled to the driveline. Hydro-pneumatic accumulators tolerate millions of charge/discharge cycles with negligible degradation and can absorb and release power at densities one to two orders of magnitude higher than current electrochemical batteries, making them particularly well suited to the high-power, short-duration transients that dominate vocational duty cycles [6]. Figure 1 illustrates this comparison graphically: for the same Class VI delivery duty cycle, a battery-based regenerative braking system recovers approximately 21% of the vehicle's kinetic energy back to acceleration, while a hydraulic system recovers approximately 71%.

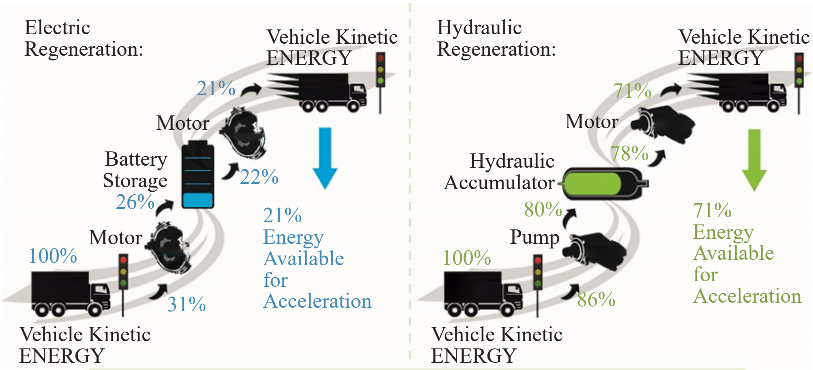

Figure 1. Comparison of regenerative-braking efficiency between an electric hybrid and a hydraulic hybrid powertrain for a Class VI delivery truck. Source: authors' own illustration based on the regenerative-braking efficiency data discussed in Section 1

Hydraulic hybridization of road vehicles is not new: experimental work dates back to the 1960s, but early systems were penalized by heavy steel accumulators and the absence of fast control electronics. Modern carbon-composite accumulators, leak-tight bent-axis variable-displacement pump/motors, low-friction biodegradable fluids and inexpensive 32-bit electronic control units have removed those barriers, and several first- and second-generation commercial systems are now in fleet service. The United States Environmental Protection Agency (EPA), in cooperation with United Parcel Service (UPS), International Truck and Engine Corporation, and Eaton, demonstrated the first full-series hydraulic hybrid Class IV delivery vehicle in 2006 and reported, under chassis-dynamometer testing, a 60-70% improvement in city fuel economy and more than 40% reduction in CO_2 relative to the conventional baseline [7], [8]. Eaton's parallel Hydraulic Launch Assist (HLA) system has accumulated more than 100 in-service refuse trucks, with first-generation units delivering approximately a 10% fuel-economy gain and a four-fold extension of brake life; the next-generation HLA, integrated with the Ultra Shift Plus transmission, is reported to provide approximately a 30% fuel-economy improvement and five-fold brake-life extension on a Peterbilt baseline [9]. Parker Hannifin's RunWise advanced series hydraulic hybrid is now offered as a turnkey Class 8 refuse-truck driveline built around the C24 bent-axis pump/motor and composite-bladder accumulators, while Bosch Rexroth markets the HRB hydrostatic regenerative braking system for vocational applications [10], [11]. A real-driving prototype hydraulic hybrid heavy commercial vehicle, instrumented with an AVL List GmbH (AVL) portable emissions measurement system, was reported in 2024 to reduce fuel consumption by up to 17% and solid-particle number concentration by 40% in stop-and-go urban routes [12].

Heavy-duty vehicles to which hydraulic hybridization is most beneficial span Federal Highway Administration Classes 4 to 8 (gross vehicle weights from approximately 6.4 to over 15 t), as shown in Figure 2. These classes encompass urban delivery vans, refuse trucks, dump trucks, transit and shuttle buses, and Class 8 tractor and vocational vehicles. The duty cycles of these vehicles are dominated by frequent acceleration and deceleration events, which makes them particularly well matched to the high-power, low-energy character of fluid-power energy storage [9].

Light-Duty		Medium Heavy-Duty				Heavy-Duty	
Class 1	Class 2	Class 3	Class 4	Class 5	Class 6	Class 7	Class 8
Less than 6,000 lb	6,000 to 10,000 lb	10,000 to 14,000 lb	14,000 to 16,000 lb	16,000 to 19,500 lb	19,500 to 26,000 lb	26,000 to 33,000 lb	Greater than 33,000 lb

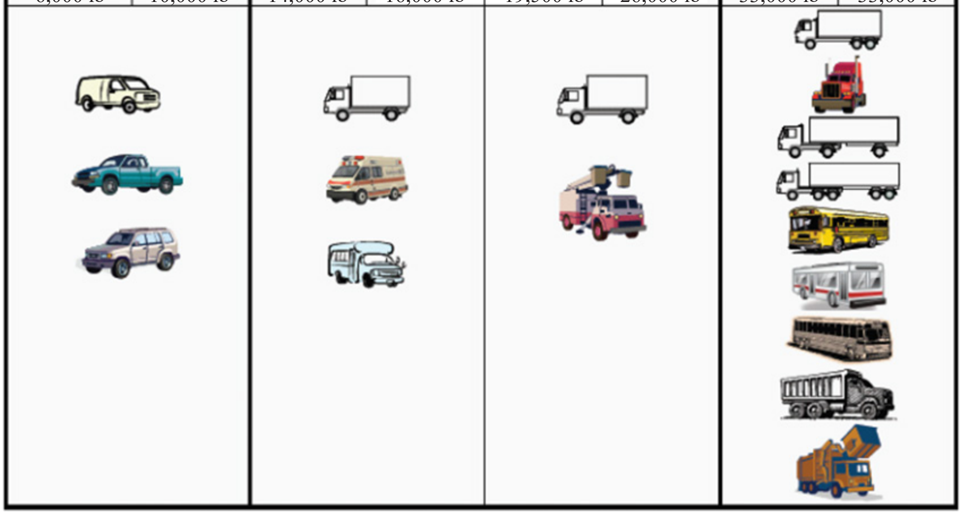

Figure 2. Federal Highway Administration vehicle weight classification (Classes 1 to 8) [4], [9]

The present study is primarily a simulation study; the review of hydraulic-hybrid architectures and demonstration systems is included only to establish the engineering context. Its specific and novel contribution is the modelling and quantitative evaluation of an air-assisted Series Hydraulic Hybrid (SHH) configuration in which a high-pressure air tank (up to 50 MPa) and a pressure exchanger are added to the conventional SHH layout, together with the option of plug-in pre-charging. The specific engineering problem that this addition is intended to solve is the intrinsically low energy density of the hydro-pneumatic accumulator: although the accumulator offers very high specific power, its limited stored energy restricts the engine-off range and the proportion of a duty cycle that can be served without firing the diesel engine. By coupling the accumulator to a high-pressure air reservoir that can be replenished either on board or from a depot during plug-in operation, the proposed configuration increases the usable stored energy and the engine-off operating fraction while retaining the high-power density and cycle durability of fluid-power components. This configuration is evaluated for a Class VI medium-duty truck over the Federal Urban Driving Schedule (FUDS) with a forward-facing closed-loop MATLAB/Simulink model developed for this work.

2. Hydraulic hybrid vehicle architectures

Three architectures dominate the published literature on hydraulic hybridization of road vehicles: the Parallel Hydraulic Hybrid (PHH), the SHH and the power-split (or compound) hydraulic hybrid. They differ in the topology by which the Internal-Combustion Engine (ICE), the hydraulic Pump/Motor (P/M) and the wheels are mechanically connected.

2.1 *PHH*

In the PHH configuration the ICE retains its conventional mechanical connection to the wheels through transmission, propeller shaft and differential, while a single variable-displacement pump/motor is coupled to the driveline, typically to the propeller shaft or the transmission output, through a clutch or a power take-off. During braking the P/M operates as a pump, transferring fluid from the low-pressure reservoir to the high-pressure accumulator and applying a retarding torque to the driveline; during acceleration the P/M operates as a motor, releasing fluid from the high-pressure accumulator and contributing to the driveline torque [13]. Figure 3 shows the conceptual layout on a typical heavy-duty chassis, and Figure 4 the corresponding schematic block diagram.

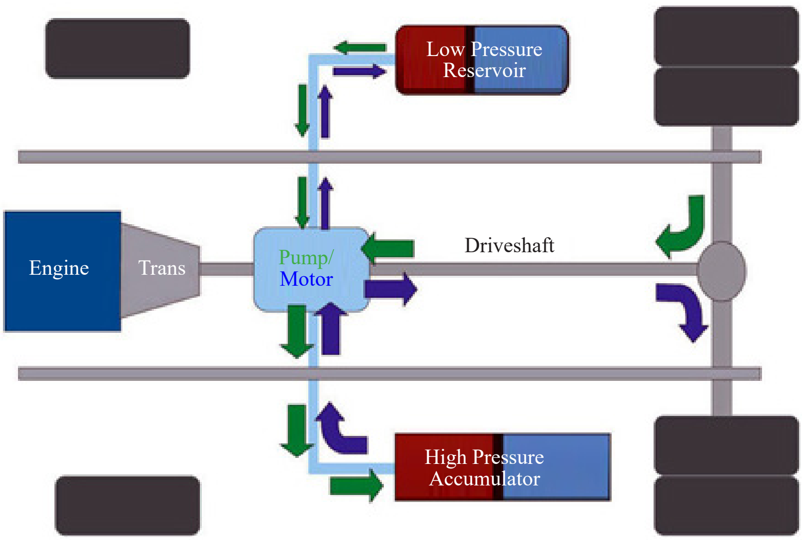

Figure 3. Conceptual layout of a PHH on a typical heavy-duty chassis

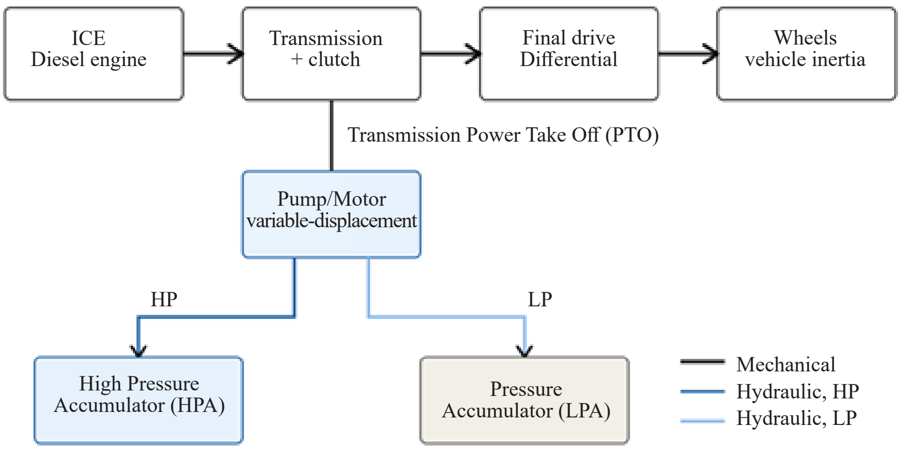

Figure 4. Schematic block diagram of the PHH architecture

The PHH is mechanically simple and can be retrofitted to existing platforms with comparatively modest re-engineering. Its main limitation is that the ICE remains coupled to the road load and therefore cannot freely choose its operating point on the Brake Specific Fuel Consumption (BSFC) map. Eaton's first-generation HLA refuse-truck system is a representative parallel architecture; reported reductions in fuel consumption range from 17% in performance mode to 28% in economy mode, with acceleration improved by approximately 26% [9].

2.2 *SHH*

In the SHH configuration the mechanical driveline is removed altogether: the ICE drives an Engine Pump/Motor (EPM) which pressurizes fluid that is delivered through high-pressure lines to one or more Drive Pump/Motors (DPM) coupled to the wheels (Figures 5 and 6). Energy storage is provided by a high-pressure accumulator placed in parallel between the EPM and the DPM, and a low-pressure accumulator (reservoir) closes the hydraulic circuit. Three design features account for the superior fuel economy of the SHH:

• regenerative braking, in which the DPM, operating as a pump, recovers more than 70% of the kinetic energy that would otherwise be lost as friction heat;

• optimum engine control, since decoupling the ICE from the wheels allows it to be operated continuously near the minimum-BSFC region of its map;

• engine off-line operation, in which the ICE is shut off whenever the energy stored in the accumulator is sufficient to satisfy the immediate power demand.

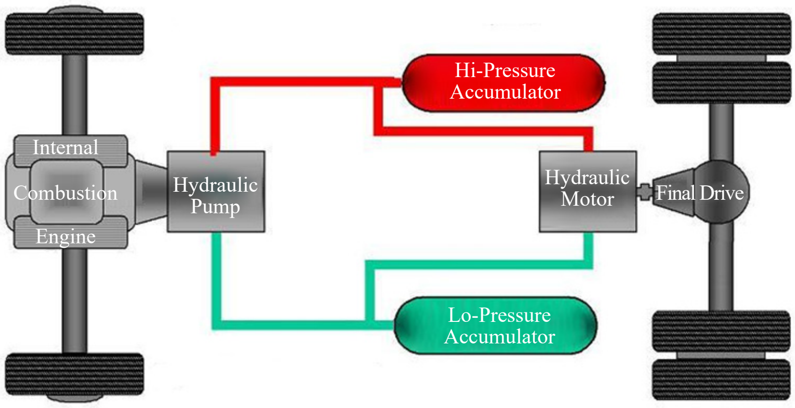

Figure 5. Conceptual layout of a SHH

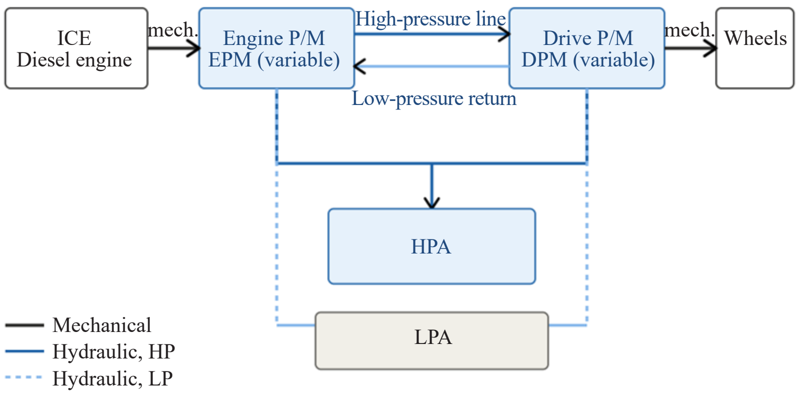

Figure 6. Schematic block diagram of the SHH architecture

Figure 7 shows the principle adapted to a passenger-car platform with a transverse engine and a single integrated EPM/DPM block, while Figure 8 shows a refuse-truck application in which the same SHH driveline is integrated into a heavy-duty chassis. The full-series EPA/UPS demonstration delivery vehicle exploited all three of the above design features and recorded, in chassis-dynamometer testing, a 60-70% city-cycle fuel-economy improvement, more than 40% CO_2 reduction, approximately 50% lower hydrocarbons and 60% lower particulate matter relative to a conventional UPS delivery van [7], [8]. Parker Hannifin's RunWise system extends the SHH concept with a power-split second range that engages a direct mechanical path above approximately 65 km/h to maintain high efficiency at cruise speeds, recovering braking energy from 65 km/h down to standstill [10].

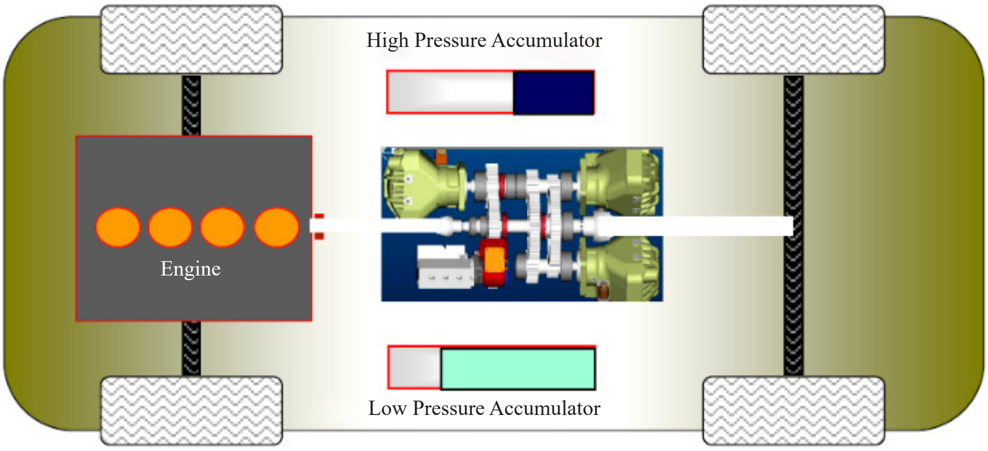

Figure 7. Detailed cross-sectional view of the SHH driveline integrated into a passenger-class chassis

Figure 8. Refuse-truck duty cycle is the canonical application for hydraulic hybridization

2.3 *Power-split (compound) hydraulic hybrid*

The power-split architecture combines the simplicity of the parallel layout at high vehicle speeds with the optimum-engine-control capability of the series layout at low and intermediate speeds (Figures 9 and 10). A two-input, two-output planetary gear set, or a clutch arrangement equivalent to it, distributes power between a hydraulic and a mechanical path. At low vehicle speeds (typically 0-65 km/h) power is transferred hydraulically; above the transition speed direct mechanical drive engages and the hydraulic path is disconnected. The two-range arrangement maintains overall transmission efficiency above 85% across most of the operating envelope [10].

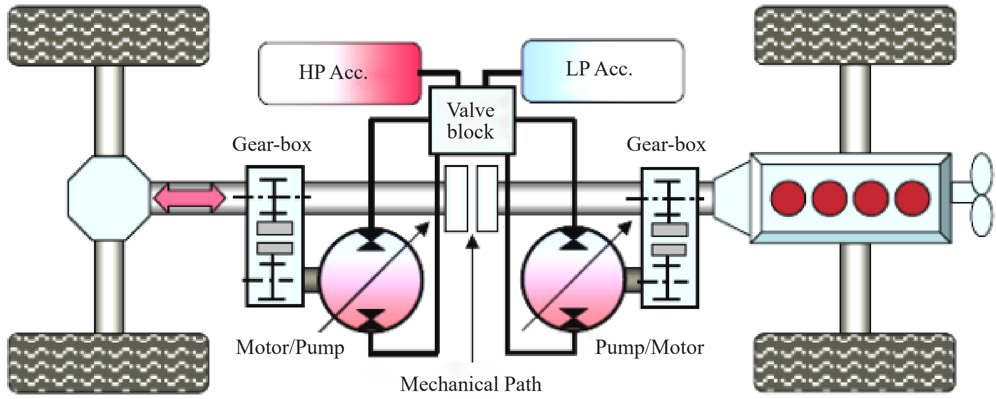

Figure 9. Conceptual layout of a power-split hydraulic hybrid

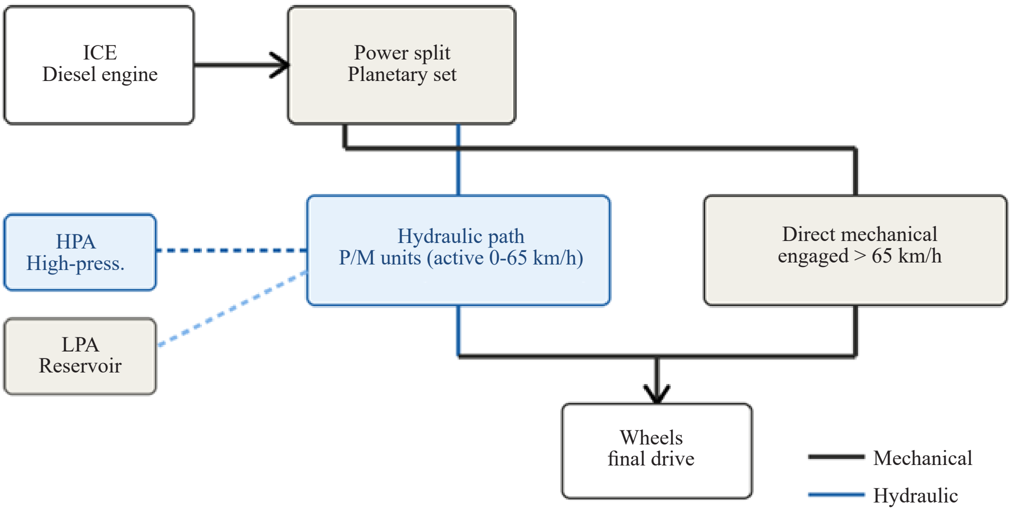

Figure 10. Schematic block diagram of the power-split (compound) hydraulic hybrid architecture

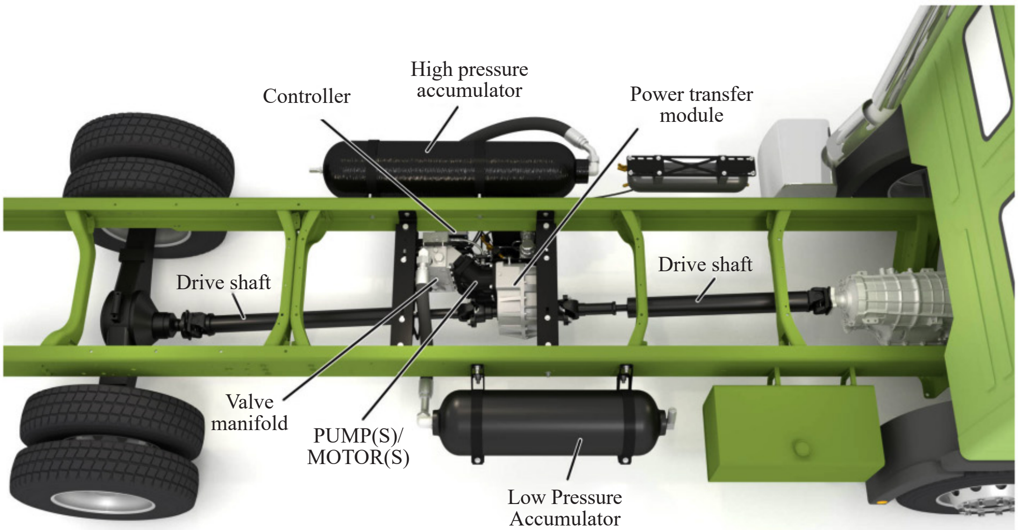

Figure 11. Hydraulic hybrid drivetrain integrated onto a Class 8 chassis

Figure 11 shows a real installation of the hybrid hardware on a Class 8 chassis, with the high-pressure accumulator running fore-and-aft along the frame rail, the pump/motor pack mounted between the propeller-shaft sections, the low-pressure accumulator transverse below the cargo body, and the valve manifold and electronic controller located on the central crossmember.

3. Sub-system dynamic models

A physically based, forward-facing closed-loop simulation model of the SHH driveline was developed in the MATLAB/Simulink environment. Figure 12 shows the high-level signal-and-power-flow diagram with central controller, engine, EPM, DPM, two-speed transmission, accumulators and wheel/vehicle dynamics, and Figure 13 shows the corresponding Simulink implementation. To increase the energy density of the accumulator and to add plug-in capability, an auxiliary high-pressure air system has been added to the basic SHH layout (Figure 14). A virtual driver, implemented as a discrete proportional-integral-derivative controller with multi-stage anti-windup, follows the FUDS speed trace by modulating the throttle and brake pedal signals. The five principal sub-models, diesel engine, hydraulic pump/motor, hydro-pneumatic accumulator, air tank with pressure exchanger and multi-stage reciprocating compressor are summarized below. The conventional baseline used for comparison is an International Class VI medium-duty truck of fully laden mass M = 7,340 kg fitted with a V8 6 L direct-injection diesel engine [14].

Throughout this paper the specific vehicle modelled is consistently a Class VI medium-duty truck, while the term heavy-duty is used only in the broader sense of Federal Highway Administration Classes 4-8 commercial vehicles, the wider category to which hydraulic hybridization is applicable.

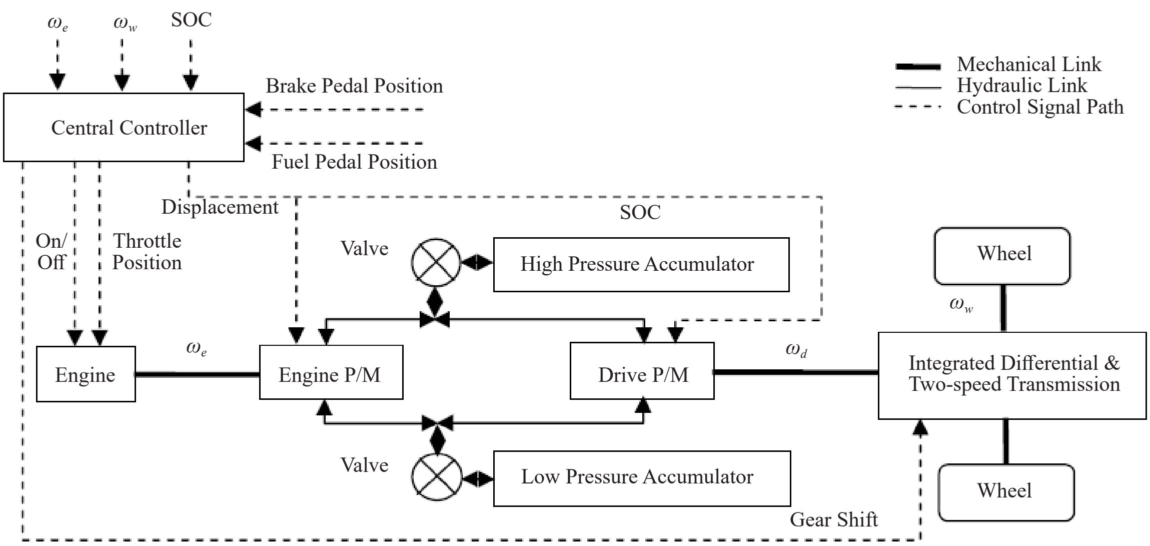

Figure 12. Block diagram of the SHH simulation model

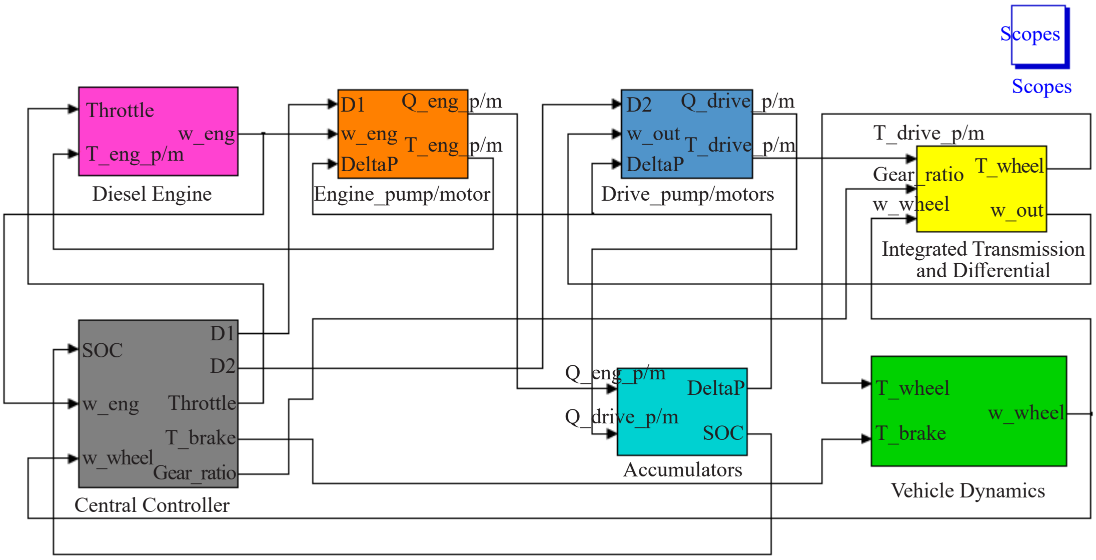

Figure 13. Forward-facing closed-loop MATLAB/Simulink implementation of the SHH model

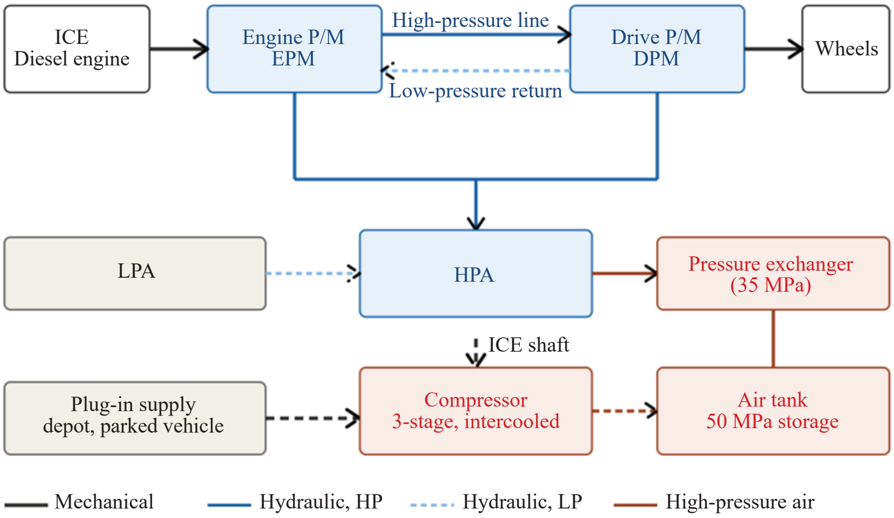

Figure 14. Schematic of the proposed air-assisted series hydraulic hybrid powertrain

3.1 *Diesel engine model*

The engine is represented by a quasi-steady, mean-value model in which the instantaneous brake torque is obtained by scaling the Wide-Open-Throttle (WOT) torque map by a non-dimensional throttle command $u \in [0, 1]$:

$$T_e(\omega_e) = uT_{e,\ \max}(\omega_e) \tag{1}$$

The WOT brake torque $T_{e,\ max}$ is taken from the BSFC map of the V8 6 L DI diesel engine measured in the W. E. Lay Automotive Laboratory at the University of Michigan [15]. Figure 15 shows the resulting BSFC contour map: the minimum-fuel-consumption island, marked by an asterisk, lies near 1,800 rpm and 580 Nm, where BSFC is approximately 214 g/kWh. The supervisory controller of the SHH (Section 5) attempts to keep the engine operating point inside the 215 g/kWh contour whenever it is fired, and to shut the engine off whenever the accumulator state of charge is sufficient to meet the next-segment power demand. The rate of change of crankshaft angular speed is governed by the lumped-inertia equation:

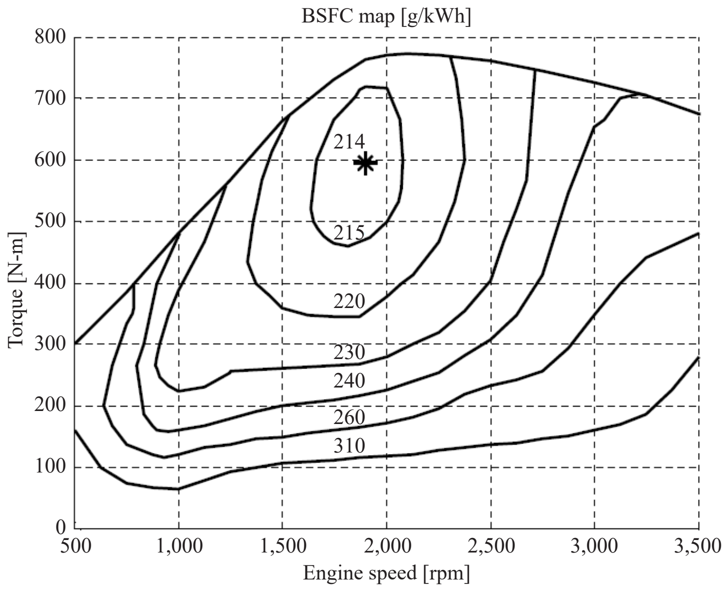

Figure 15. BSFC map of the V8 6 L DI diesel engine used as the prime mover in the SHH simulation [15]

$$\left(J_e + J_{epm}\right)\frac{\mathrm{d}\omega_e}{\mathrm{d}t} = T_e\left(\omega_e\right) - T_{epm}\left(\omega_e\right) \tag{2}$$

where J_e and J_{epm} are the engine and engine-pump/motor inertias and T_{epm} is the load torque imposed by the EPM. A logic block forces the engine torque to zero whenever the engine speed exceeds the rated maximum, and a separate supervisory module commands engine shut-off whenever the SHH accumulator state-of-charge is sufficient to meet the predicted next-segment demand.

3.2 *Hydraulic pump/motor model*

Bent-axis axial-piston machines are used in this study because they combine high power density with the wide dynamic range of variable displacement. The ideal volumetric flow rate and shaft torque are:

$$Q_i = x\omega D \tag{3}$$

$$T_i = xpD \tag{4}$$

where $x \in [-1, 1]$ is the displacement factor (positive in motor mode, negative in pump mode), ω is the shaft angular speed, D is the maximum geometric displacement per radian, and p is the pressure differential across the unit. The actual flow and torque differ from the ideal values because of internal leakage, viscous and Coulomb friction, hydrodynamic losses and compressibility effects. Following the updated Wilson model [16], the volumetric and torque efficiencies of the unit operating in pump mode are:

$$\eta_{v,\,pump} = \frac{Q_a}{Q_i} = 1 - \frac{C_s}{|x|\sigma} - \frac{\Delta p}{\beta}\frac{C_{st}}{|x|\sigma} \tag{5}$$

$$\eta_{t,\,pump} = \frac{T_i}{T_a} = \frac{1}{1 + \frac{C_v \sigma}{|x|} + \frac{C_f}{|x|} + C_h x^2 \sigma^2} \tag{6}$$

where σ is the rotational reduction factor and the loss coefficients C_s, C_{st}, C_v, C_f and C_h account respectively for laminar slip, turbulent slip, viscous friction, Coulomb friction and hydrodynamic friction. Their calibrated numerical values to match the EPA reference machine [15], [16] are summarized in Table 1.

Table 1. Constants and calibrated loss coefficients for the bent-axis pump/motor model

Parameter	Value	Parameter	Value
β (bulk modulus)	1,660 MPa	C_s (laminar slip)	2.627×10^{-9}
μ (dynamic viscosity)	0.034 N · s/m^2	C_{st} (turbulent slip)	1.332×10^{-7}
ρ (density)	850 kg/m^3	C_v (viscous friction)	1.2×10^{-4}
C_f (Coulomb friction)	1.005×10^{-2}	C_h (hydrodynamic)	19.8

Figures 16 and 17 plot the resulting total efficiency contours of the pump/motor as a function of displacement factor x and shaft speed for system pressures of 14 MPa and 28 MPa, respectively. At both pressures the unit operates above 0.92 over a broad region of the (x, ω) plane, peaking near 0.96 at large displacement and intermediate speeds. Operation at small displacement factors ($x < 0.3$) is to be avoided whenever possible because efficiency degrades sharply, particularly at high speed. This finding has direct implications for the supervisory power-management strategy discussed in Section 5: the controller is designed to favor high-displacement, lightly loaded operation rather than low-displacement, heavily loaded operation.

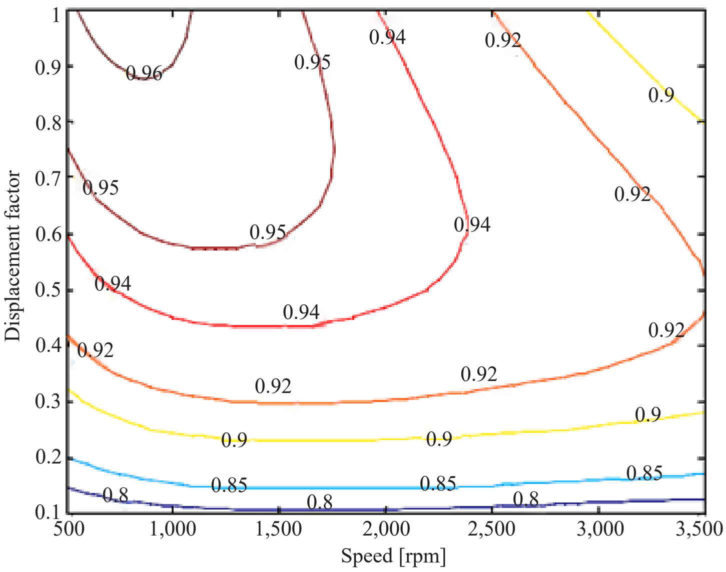

Figure 16. Total efficiency contour map of the bent-axis pump/motor at 14 MPa system pressure

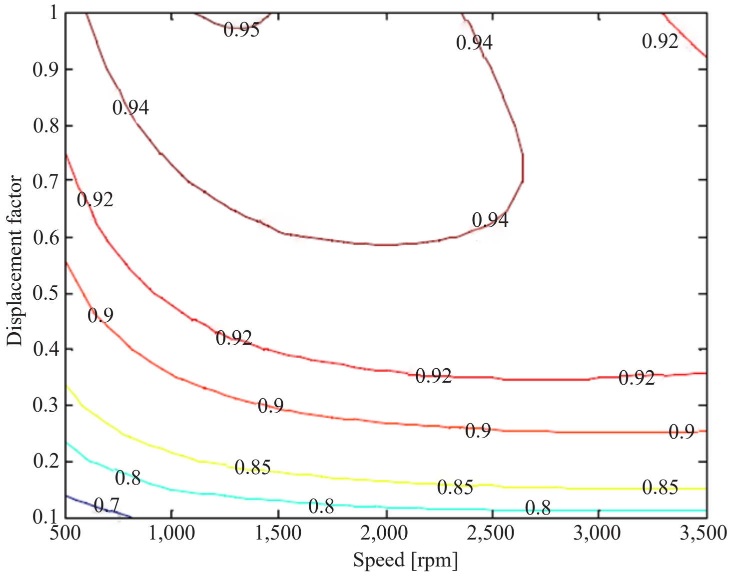

Figure 17. Total efficiency contour map of the same pump/motor at 28 MPa

3.3 *Hydro-pneumatic accumulator model*

The high-pressure accumulator stores energy by compressing a pre-charged inert gas (typically nitrogen) separated from the working fluid by an elastomeric bladder lined with foam to suppress thermal losses. Under the assumption that the gas obeys the polytropic relation:

$$PV^k = C \tag{7}$$

where k is the polytropic index (1.0 for an ideal isothermal process, 1.4 for an adiabatic ideal-gas process) and C is a constant determined by the pre-charge pressure and volume. Modern composite bladder accumulators with elastomeric foam insulation transfer very little heat to the surroundings during a typical hybrid duty cycle, so an adiabatic value of $k = 1.4$ is used in this work [18]. Internal frictional losses are accounted for by deducting a pressure drop proportional to the ratio of cumulative friction loss to cumulative input energy from the gas pressure.

For real hydro-pneumatic accumulators the effective polytropic index typically lies in the range $k = 1.2$-1.4, the lower bound corresponding to appreciable gas-to-wall heat exchange and the upper bound to a fully adiabatic compression. In the present model heat exchange between the gas and the environment is neglected and the adiabatic limit $k = 1.4$ is adopted, an assumption justified by the foam-lined composite bladder, which suppresses convective heat transfer during the short charge/discharge transients of an urban duty cycle. The high-pressure accumulator is modelled with a nitrogen pre-charge pressure of 12.5 MPa, a maximum working pressure of 35 MPa and a nominal gas volume of 32 L; these values are consistent with, and bracket, the 14 MPa and 28 MPa operating points used for the pump/motor efficiency maps of Figures 16 and 17.

3.4 *Air-tank and pressure-exchanger models*

As shown in Figure 14, a high-pressure air tank stores compressed air at up to 50 MPa and is connected to the high-pressure accumulator through a pressure exchanger. Provided that the tank is sufficiently large for its temperature to remain essentially constant, the energy stored in the air tank can be expressed for an isothermal process with an ideal gas, such as:

$$E = mRT\ln\left(\frac{P}{P_0}\right) \tag{8}$$

where m is the air mass in the tank, R is the specific gas constant for air, T is the absolute temperature, P is the air-tank pressure and P_0 is the atmospheric reference pressure. Each switching event from the high-pressure to the low-pressure side of the pressure exchanger releases the residual mass:

$$m_{loss} = \rho V_{PE} \tag{9}$$

where V_{PE} is the pressure-exchanger volume; the cumulative loss after N switches is $m_{loss} = N \cdot \rho \cdot V_{PE}$, and the corresponding energy loss is computed from an isothermal expansion equation analogous to equation (8).

3.5 *Multi-stage compressor model*

When the air-tank pressure falls below a threshold P_{min}, a three-stage reciprocating compressor (Figure 18) driven either by an external electric motor (during plug-in operation) or by the on-board ICE (during running operation) recharges the tank. Three-stage compression with intercooling is preferred to single-stage compression because it approaches the ideal isothermal characteristic and reduces both the work input per cycle and the discharge temperature, the latter being critical for lubricant durability [19]. Figure 19 illustrates this on the P-V diagram: the shaded area between the three-stage curve a-b-c-d-e-f-g-h and the ideal isothermal curve a-b-j-h is the work saved per cycle relative to a single-stage adiabatic compression a-b-c-k-h. For the ICE-driven case the compressor displacement per revolution V_{cs} rotates at the engine angular speed ω_e so that the mass-flow rate is $\rho \cdot V_{cs} \cdot \omega_e/(2\pi)$. The compression work per cycle, neglecting clearance volume and assuming adiabatic compression, is:

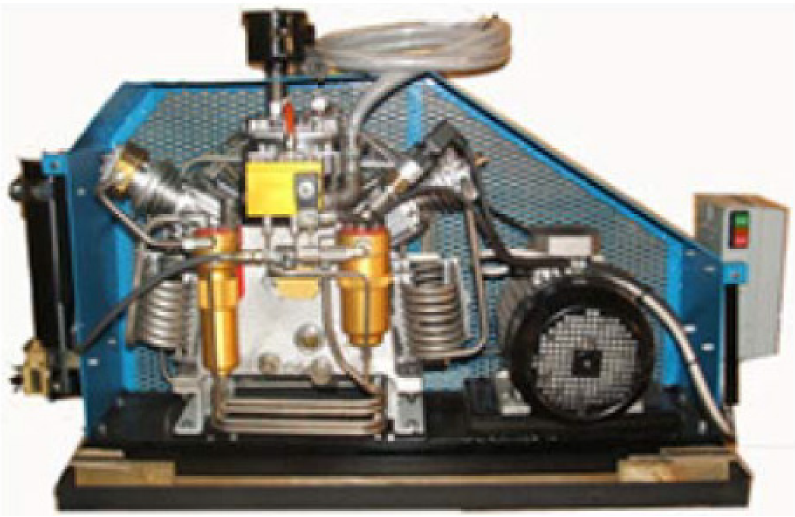

Figure 18. Commercial high-pressure (50 MPa) three-stage reciprocating compressor of the type used to recharge the auxiliary air tank in the proposed air-assisted SHH driveline (Figure 14)

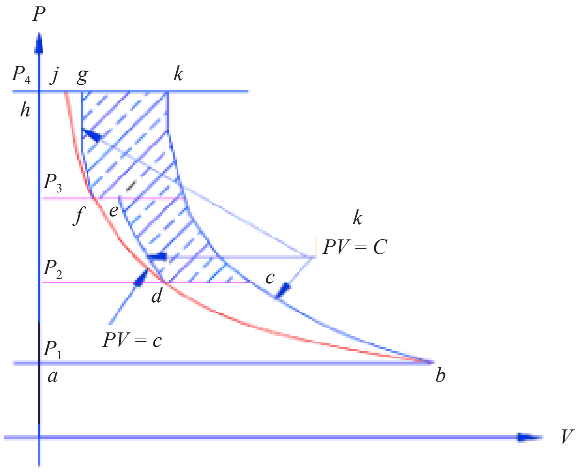

Figure 19. *P-V* diagram for a three-stage reciprocating compressor without clearance volume

$$W_c = \frac{k}{k-1}\frac{n_s p_1 V_1}{\eta_c}\left[\left(\frac{P_4}{P_1}\right)^{\frac{k-1}{kn_s}} - 1\right] \tag{10}$$

where $n_s = 3$ is the number of compression stages, P_1 and P_4 are respectively the inlet (atmospheric) and outlet (tank) pressures, and η_c is the overall compressor efficiency, taken here as 0.80 to lump together the mechanical and thermodynamic loss components [17], [19].

4. Energy recovery efficiency analysis

4.1 *Vehicle dynamics and required power*

The vehicle is represented as a single mass *M* lumped at the center of gravity and moving longitudinally on a smooth road. Lateral, pitch, yaw and roll motions are neglected, so the resistive force at the wheels is the sum of the rolling-resistance, aerodynamic-drag and gradient terms. The rolling-resistance term is derived from the free-body diagram of Figure 20: a deformable wheel of radius r supports a normal load equal to the vehicle weight component on that wheel, and the deformation creates an offset b between the line of action of the normal reaction and the wheel center, producing a backward force $F = N \cdot b/r$ where the dimensionless rolling-resistance coefficient is $C_{rr} = b/r$. The road load can therefore be written:

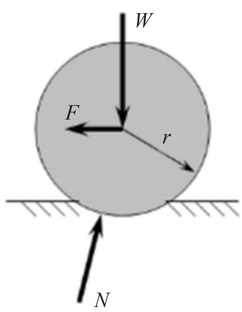

Figure 20. Free-body diagram of a deformable wheel rolling on a soft surface [20]

$$R_L = Mgf\cos\theta + 0.5\rho_a C_D A V^2 + Mg\sin\theta \tag{11}$$

where g is the gravitational acceleration, f the rolling-resistance coefficient, ρ_a the air density, C_D the drag coefficient, A the frontal area, V the vehicle speed and θ the road grade angle. The instantaneous power required at the wheels to overcome the road load and accelerate the vehicle is:

$$\dot{W}_{req} = R_L V + (M + M_r) a V \tag{12}$$

where the equivalent mass of the rotating components M_r includes the gear ratios for the final drive and transmission. When the vehicle is propelled exclusively by the hydraulic motor (transmission gear ratio set to zero), M_r is recomputed without the transmission contribution.

4.2 *Theoretical and real recovery efficiency*

The theoretical regenerative-braking efficiency is defined as the ratio of the kinetic energy stored during braking to the kinetic energy supplied during the preceding driving phase:

$$\left(\frac{E_b}{E_d}\right)_{theo} = \frac{F_B V t_B}{F_D V t_D} \tag{13}$$

The real, component-loss-corrected efficiency is obtained by multiplying the theoretical value by the round-trip efficiencies of the energy-storage device (η_{es}), the power control circuitry (η_{pc}), the pump/motor ($\eta_{p/m}$) and the mechanical gearing (η_{mg}). Because each component is traversed twice (once during charging and once during discharging), the corresponding efficiencies appear squared:

$$\left(\frac{E_b}{E_d}\right)_{real} = \left(\frac{E_b}{E_d}\right)_{theo} \eta_{es}^2 \eta_{pc}^2 \eta_{p/m}^2 \eta_{mg}^2 \tag{14}$$

Equation (14) shows that even modest improvements in any of the round-trip efficiencies are amplified twice in the overall recovery, justifying the considerable engineering effort that has been devoted to high-efficiency bent-axis pump/motors, low-loss accumulator bladders and variable hydraulic transformers in the recent literature [20], [21].

4.3 *Simulation results on the FUDS cycle*

Tables 2 and 3 summarize the theoretical and real recovery efficiencies obtained for three peak vehicle speeds (8, 14 and 25 km/h) representative of urban refuse-collection, urban-delivery and mixed-urban duty cycles, respectively, and for two values of the cruise-to-total time ratio t_{cs}/t_t (0 and 0.4). The acceleration phase length is held constant. Figure 21 plots the same data graphically.

These three peak speeds were not chosen arbitrarily: the FUDS trace is composed of a sequence of accelerate-cruise-decelerate micro-trips whose peak speeds span this range, so 8, 14 and 25 km/h represent, respectively, the low-speed refuse-collection micro-trips, the intermediate urban-delivery micro-trips and the upper-bound mixed-urban micro-trips that together make up the complete cycle. The two cruise-to-total-time ratios bracket the limiting cases of pure stop-and-go operation ($t_{cs}/t_t = 0$) and a representative urban cycle in which 40% of the time is spent cruising ($t_{cs}/t_t = 0.4$); evaluating the recovery efficiency at these end-members therefore brackets the performance expected across the full FUDS schedule.

Table 2. Theoretical recovery efficiency $(E_b/E_d)_{theo}$ for three peak speeds and two cruise/total-time ratios

Peak speed (km/h)	$t_{cs}/t_t = 0$	$t_{cs}/t_t = 0.4$
8	0.7895	0.2858
14	0.8631	0.3231
25	0.8889	0.3369

Table 3. Real (component-loss-corrected) recovery efficiency $(E_b/E_d)_{real}$ for the same operating points, computed with $\eta_{es} = 0.92$, $\eta_{pc} = 0.95$, $\eta_p/m = 0.93$, $\eta_{mg} = 0.97$

Peak speed (km/h)	$t_{cs}/t_t = 0$	$t_{cs}/t_t = 0.4$
8	0.5456	0.1975
14	0.5964	0.2233
25	0.6142	0.2328

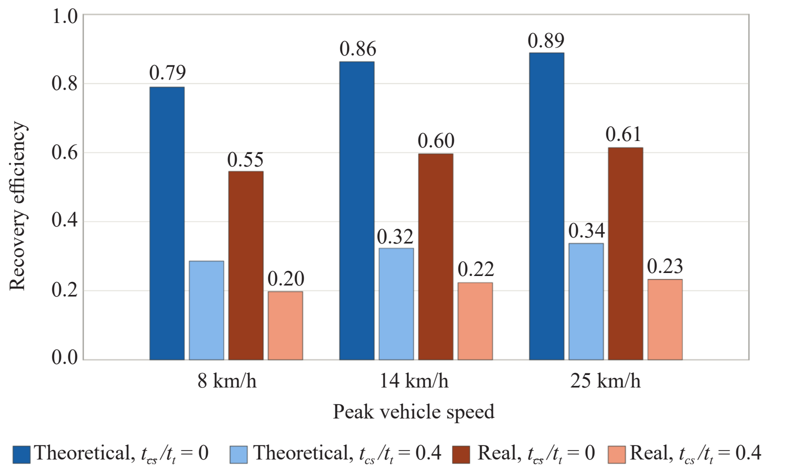

Figure 21. Theoretical and real (component-loss-corrected) regenerative-braking recovery efficiencies for the air-assisted SHH driveline

Three observations follow from these results. First, the theoretical recovery efficiency increases monotonically with peak speed, from 0.79 at 8 km/h to 0.89 at 25 km/h in the pure stop-and-go case, because a larger fraction of the input energy resides in kinetic form rather than being dissipated against rolling and aerodynamic resistance. Second, the addition of a cruise segment of length equal to 40% of the total cycle time ($t_{cs}/t_t = 0.4$) reduces the recoverable fraction by approximately a factor of three, because energy expended overcoming road load during the cruise segment cannot be regenerated. Third, application of the round-trip component efficiencies reduces the practically attainable recovery to 0.55-0.61 in the pure stop-and-go case and to 0.20-0.23 in the mixed cycle. These figures are consistent with the 60-70% city-cycle fuel-economy improvement reported by the EPA for the full-series UPS demonstration vehicle [7] and with the 17% real-driving fuel-consumption reduction measured on a Euro IV diesel truck retrofitted with a parallel hydraulic hybrid driveline by Surawski and co-workers [12].

Although a dedicated experimental test rig was beyond the scope of this work, the model can be validated against published field data. The simulated real recovery of 0.55-0.61 in the pure stop-and-go case corresponds to the upper part of the 60-70% city-cycle fuel-economy improvement reported by the EPA for the full-series UPS Class IV demonstration vehicle [7], [8], whereas the degraded recovery of 0.20-0.23 once a 40% cruise segment is introduced is consistent with the ≈ 17% real-driving fuel-consumption reduction measured by Surawski and co-workers on a parallel hydraulic-hybrid truck whose routes include cruise segments [12]. The agreement in both magnitude and trend between the simulation outputs and these independent field measurements supports the validity of the model in the absence of a purpose-built experiment.

A first-order sensitivity assessment follows directly from Equation (14): because each of the four round-trip efficiencies enters squared, the real recovery efficiency is most sensitive to the pump/motor efficiency and the energy-storage efficiency. A ±2% absolute change in any single component efficiency produces an approximately ±4% change in the recovered-energy fraction, and simultaneous ±2% variations in all four components produce an approximately ±15% spread, while the cruise-to-total-time ratio remains the dominant operational sensitivity, reducing recovery by roughly a factor of three between $t_{cs}/t_t = 0$ and 0.4. A full probabilistic (Monte-Carlo) sensitivity and uncertainty analysis over the complete parameter set is identified as future work.

5. Supervisory power-management strategy

The supervisory controller of Figure 12 must distribute the driver-demanded power $\dot{W}_{req}$ between the ICE and the hydraulic P/M while respecting the displacement, accumulator state-of-charge, engine speed and emission constraints. Two operating modes are distinguished.

Algorithm 1. Rule-based power-distribution logic, executed at every simulation time step.

1: compute driver-demanded power W_{req}
2: if $W_{req} > 0$ (traction) then
3: deliver $W_h = min(W_{req}, W_{h,max})$ from the hydraulic motor
4: if $W_h < W_{req}$ then fire engine: $W_e = (W_{req} - W_h)/(\eta_h \cdot \eta_t) + W_c$
5: else keep the engine off or idling (drive only the air compressor)
6: else if $W_{req} < 0$ (braking) then
7: if SOC < SOC_{max} then charge accumulator: $W_p = min(|W_{req}|, W_{p,\,max})$
8: apply the friction brake for the remainder: $W_{fric} = |W_{req}| - W_p$
9: end if
10: update accumulator state-of-charge and air-tank pressure

5.1 *Power-delivery (traction) mode*

When the driver requests positive power ($\dot{W}_{req} > 0$) the strategy first attempts to satisfy the demand entirely from the hydraulic motor, allowing the engine to idle or to drive only the air compressor. The actual hydraulic power delivered is:

$$\dot{W}_{h,\,act} = Q_{act} \Delta p \eta_{p/m,\,m} \tag{15}$$

Where $Q_{act} = D_{act} \cdot \omega_h$ is the actual volumetric flow rate, $D_{act} \in [D_{min}, D_{max}]$ is the actual displacement, Δp is the pressure differential and $\eta_{p/m,\,m}$ is the motor-mode total efficiency. If the maximum hydraulic power is insufficient to satisfy the demand, the engine makes up the deficit through the EPM:

$$\dot{W}_e = \frac{\dot{W}_{req}}{\eta_h \eta_t} - \dot{W}_{h,\,act} + \dot{W}_c \tag{16}$$

Where η_h and η_t are respectively the hydraulic-transmission and the mechanical-transmission efficiencies and $\dot{W}_c$ is the air-compressor power demand.

5.2 *Power-absorption mode*

During deceleration ($\dot{W}_{req} < 0$) the engine is shut off or operated only to drive the compressor, and the P/M operates as a pump to charge the accumulator. The same displacement limits and accumulator state-of-charge constraints apply; if the braking demand exceeds the maximum pump capacity or the accumulator becomes fully charged, the friction brakes are activated to dissipate the excess energy as heat:

$$\dot{W}_{fric} = \dot{W}_{req} - \dot{W}_{p,\,act} \tag{15}$$

5.3 *Recent advances in supervisory control*

The simple rule-based strategy described above leaves significant fuel-economy improvements unrealized because it does not anticipate the future load profile. Three families of more sophisticated strategies have appeared in the literature since 2018:

• Equivalent Consumption Minimization Strategy (ECMS) and adaptive ECMS, in which an instantaneous Hamiltonian assigns equivalent fuel cost to the use of stored hydraulic energy and the optimization is performed at every time step. Wang and co-workers developed rule-based strategy and extended ECMS to a parallel electro-hydraulic hybrid wheel loader and reported energy-use gaps of only 2.99% (simulation) and 6.10% (experiment) relative to the global-optimum dynamic-programming benchmark [22].

• Dynamic programming and Pontryagin-minimum-principal solutions, used as benchmarks but typically too computationally heavy for on-board use.

• Learning-based strategies, including fuzzy-logic controllers, artificial neural networks and reinforcement-learning agents trained on representative duty cycles. Liu and co-workers reviewed these methods for electro-hydraulic hybrid powertrains and identified the principal open challenges as multi-mode coordination, mode-transition smoothness and online adaptation to drift in vehicle parameters [23].

More recent literature (2024-2026) continues to advance these directions. Huang and co-workers [24] provide a comprehensive review of artificial-intelligence-based energy-management strategies for hybrid powertrains, classifying them into knowledge-driven, data-driven, reinforcement-learning and hybrid paradigms. Abdelbaky and co-workers [25] developed and optimized, in a MATLAB/Simulink environment, a series-parallel hybrid powertrain for a van-style commercial vehicle, tuning the supervisory controller with genetic-algorithm and particle-swarm optimisation to improve fuel economy, an approach closely related to the forward-facing Simulink model used in the present work. For regenerative braking specifically, Szumska [26] reviewed system design, control strategies and energy-storage technologies, including hydro-pneumatic accumulators, for kinetic-energy recovery, while Ahmed and co-workers [27] proposed an energy-management and power-distribution strategy for a battery/ultracapacitor hybrid energy-storage system with regenerative-braking control. These recent studies reinforce the trends discussed above and situate the present air-assisted hydraulic hybrid within the broader movement toward intelligent, multi-source energy management.

In the present work the proposed air-assisted SHH configuration is operated exclusively with the rule-based strategy of Algorithm 1; the ECMS, dynamic-programming and learning-based strategies surveyed above have not yet been applied to this specific configuration and are identified as future work.

6. Commercial and demonstration systems

Several commercial and pre-commercial hydraulic hybrid systems are now in fleet service or in advanced demonstration. Figure 22 shows the real installation of a parallel hydraulic hybrid retrofit system on the underside of a Class 6 delivery truck, with the drive shaft passing through the central pump/motor and the high-and low-pressure accumulators visible above and below it (image adapted by the authors from manufacturer retrofit documentation). Table 4 summarizes the salient characteristics and reported fuel savings of these systems.

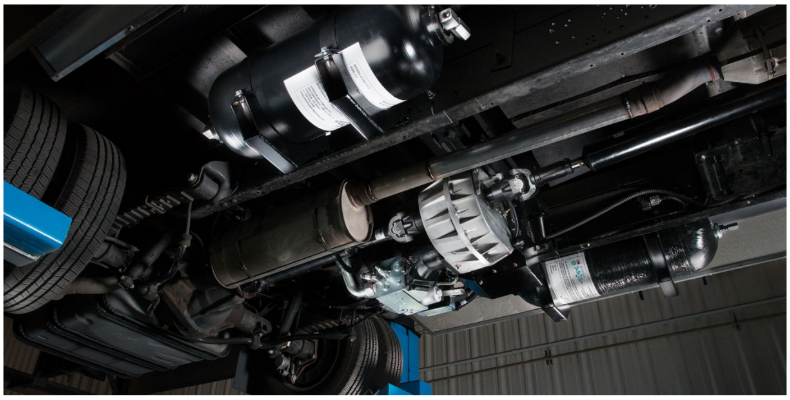

Figure 22. Real installation of a parallel hydraulic hybrid retrofit kit on the underside of a Class 6 delivery truck

Table 4. Principal commercial and demonstration hydraulic hybrid systems (status as reported between 2014 and 2024)

System	Architecture	Application	Reported fuel saving	Ref.
Eaton HLA (1st gen.)	Parallel	Refuse trucks	9-10% fuel; 4 × brake life	[9]
Eaton HLA (2nd gen.) + Ultra Shift	Parallel	Refuse trucks	≈ 23% fuel; 5 × brake life	[9]
Parker RunWise	Series + power split	Class 8 refuse	Up to 50% city cycle	[10], [11]
EPA/UPS/Eaton/Int'l	Full series	Class IV delivery	60-70% city economy; > 40% CO_2	[7], [8]
Bosch Rexroth HRB	Parallel (regen.)	Vocational	≈ 25% city cycle	[11]
Lightning Hybrids retrofit	Parallel	MD trucks 6.4-18 t	Up to 35% heavy cycles	[6]
Dana Spicer PowerBoost	Parallel integrated	On/off highway	20-25% off-highway	[6]
Real-driving prototype	Parallel	Euro IV diesel truck	17% fuel; 40% PN reduction	[12]

7. Emerging electro-hydraulic hybrid architectures

Although hydraulic hybridization alone is incompatible with the zero-tailpipe-emission targets that the European Union and the State of California have set for new urban buses (100 % by 2035) and for many vocational vehicle classes by 2040, the very high specific power and cycle durability of the hydro-pneumatic accumulator make it an attractive complement to a battery-electric or fuel-cell traction system. Two configurations have received the most attention in the recent literature [23]:

• Series Electro-Hydraulic Hybrid (S-EHHV), in which a battery and an electric machine constitute the primary energy source while a hydro-pneumatic accumulator and a hydraulic pump/motor handle the high-power, short-duration transients of acceleration and braking. The accumulator absorbs the peaks of regenerative braking that would otherwise be discarded by the battery management system and protects the battery from damaging C-rates.

• Mechanical-Electric-Hydraulic Power-Coupling (MEHPC) systems, in which a planetary gear set or an equivalent power-split arrangement combines a permanent-magnet rotary motor and a swashplate axial-piston pump/motor, allowing simultaneous transformation between electrical, mechanical and hydraulic energy [23], [28]. Table 5 summarizes, at qualitative and order-of-magnitude level, how the pure-electric, pure-hydraulic and electro-hydraulic approaches compare in terms of specific power, energy density, urban braking-energy recovery, storage cycle life, incremental cost and best-suited duty.

The motivation for these hybrid-of-hybrids architectures is shown clearly by Figure 1 in Section 1: the round-trip efficiency of a battery-only regenerative-braking system on a heavy-duty Class VI duty cycle is approximately 21%, while that of a hydro-pneumatic system is 71%, a more than three-fold gap that is not easily closed by improvements in battery cell chemistry or power electronics alone. Figure 23 shows a representative example of an electric-hybrid drivetrain layout for a passenger-class vehicle: the same chassis volume can in principle accommodate both a downsized lithium-ion battery and a small hydro-pneumatic accumulator, with the electric machine handling continuous traction and the hydraulic machine handling the high-power transients.

Table 5. Order-of-magnitude and qualitative comparison of pure-electric, pure-hydraulic and electro-hydraulic energy-recovery systems for heavy-duty vehicles (values compiled from the cited literature; qualitative or order-of-magnitude where exact figures are not available)

Metric	Pure electric (battery)	Pure hydraulic (HHV)	Electro-hydraulic (EHHV)
Specific power	Moderate	Very high (1-2 orders > battery) [6]	High
Energy density	High	Low	High (battery-dominated)
Urban braking-energy recovery	≈ 21% (Figure 1)	≈ 71% (Figure 1)	≈ 71% on transients [29]
Storage cycle life	Limited under deep cycling [5]	> 10^6 cycles [6]	Battery SoH extended ≈ 3% [29]
Relative incremental cost	High (rare-earth, Cu) [11]	Low (commodity materials) [11]	Moderate
Best-suited duty	Continuous traction	High-power transients	Combined urban duty

Recent experimental work on hybrid hydraulic excavators has demonstrated that the combination of a planetary-gear power split, a hydrostatic transmission and an extremum-seeking energy-management strategy can reduce overall energy consumption by approximately 10% and improve regenerative recovery by approximately 48% compared with conventional baselines, while also extending battery state-of-health by approximately 3% over a projected 50,000 working cycles [29], [30]. Comparable electro-hydraulic concepts have been investigated for parallel-hybrid wheel loaders [22] and for urban-bus applications, where the hydraulic accumulator captures the braking-energy peaks that would otherwise saturate the battery management system [23].

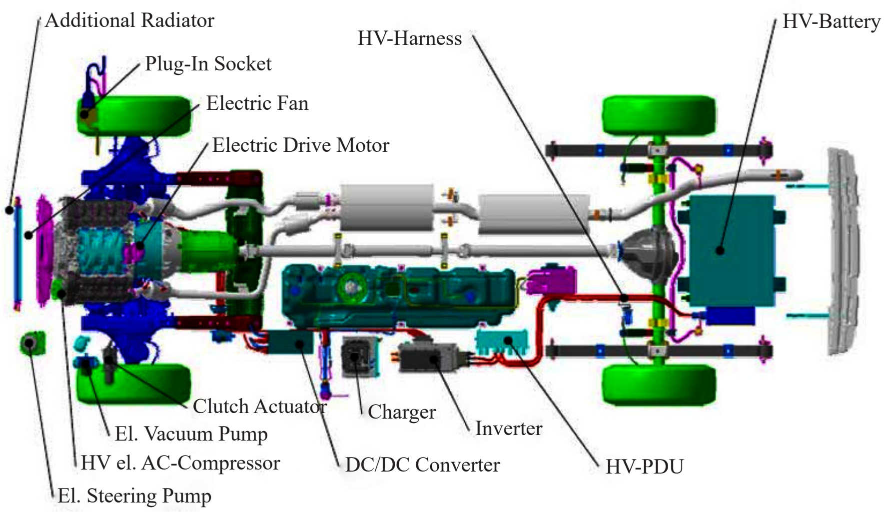

Figure 23. Representative layout of a hybrid-electric powertrain showing the locations of the high-voltage battery, drive motor, inverter, charger and DC/DC converter. Source: authors' own illustration

8. Cost and economic viability

Hydraulic hybrid systems use commodity materials-steel, carbon-fiber overwrap, mineral-based or biodegradable hydraulic fluid, copper-free composite bladders-whose cost has been comparatively stable over the last decade, in contrast to the rare-earth metals and battery-grade copper used in lithium-ion packs [11]. The EPA estimates the long-term incremental manufacturing cost of a fully developed hydraulic Class IV delivery vehicle at approximately USD 7,000 above the conventional baseline, against estimated lifetime fuel and brake-maintenance savings exceeding USD 50,000 over a typical 20-year fleet service life [7].

For the Class VI medium-duty truck investigated in this paper, the projected incremental capital expenditure of the parallel hydraulic hybrid configuration is approximately the difference between USD 45,000 (conventional) and USD 75,000 (hydraulic hybrid), or USD 30,000. With reported annual fuel-cost savings of the order of USD 4,000-6,000 (varying with regional Diesel prices) and a brake-pad replacement interval extended from 90 days to 5-6 years, the simple payback period is approximately 4-5 years for vehicles operating at least 100,000 km per year, and the system also reduces fleet CO_2 emissions by approximately 40-50 t per vehicle per year. These figures are consistent with the cost-benefit analyses reported by the California Energy Commission for the RunWise series-hybrid Class 8 refuse truck [11] and with the financial analyses presented for first- and second-generation Eaton HLA installations [9].

Quantitatively, because tank-to-wheel CO_2 scales almost linearly with diesel consumption (emission factor ≈ 2.68 kg CO_2 per litre of diesel), the 17-35% fuel-consumption reductions documented here and in the cited demonstrations translate into proportional 17-35% reductions in tank-to-wheel CO_2, in addition to the 40% reduction in solid-particle-number concentration measured on a real-driving hydraulic-hybrid truck [12] and the more than 40% CO_2 reduction reported for the EPA/UPS full-series demonstration [7].

9. Discussion

The simulation and demonstration results reviewed in this paper confirm that hydraulic hybridization is most attractive when three conditions are simultaneously satisfied: a vehicle of large gross mass, a duty cycle dominated by frequent stop-and-start events, and a service life sufficient to amortize the incremental capital cost. Refuse trucks (Figure 8), urban delivery vans (Figure 22), transit buses and construction machinery satisfy all three, and it is in those segments that commercial deployment is now most advanced. Long-haul tractor-trailer operations, by contrast, do not benefit appreciably from hydraulic hybridization because the cruise share of the duty cycle is too high and the kinetic-energy share that can be recovered is correspondingly small. This conclusion is unchanged from the original 2014-2015 modelling work but is now supported by considerably more demonstration data, including the 2024 real-driving emissions campaign of Surawski and co-workers [12] and the cumulative more-than-100-vehicle in-service experience of the Eaton HLA program [9].

Three open research questions remain. First, supervisory control strategies that combine model-based optimization (ECMS, dynamic programming) with machine-learning components capable of online adaptation to the local duty cycle are still in their infancy for hydraulic hybrids; published work in this area is dominated by hybrid-electric powertrains. Second, integration of the hydro-pneumatic accumulator with a battery-electric or fuel-cell traction system in an electro-hydraulic hybrid architecture offers a credible pathway to satisfy the 90% CO_2 reduction target of EU Regulation 2024/1610 while preserving the high specific power and cycle durability of fluid-power components, but reliability and safety standards specific to such multi-energy-source systems have not yet been fully developed. Third, plug-in pre-charging of the air tank or the high-pressure accumulator, a feature explored in the air-assisted SHH variant simulated in Section 4, could reduce on-board fuel consumption to near-zero on the first kilometers of a fleet shift, but its commercial uptake is contingent on the availability of compressed-air or high-pressure-fluid charging infrastructure at depots, an aspect that has received very little attention in the public literature.

Finally, although the fuel-economy gains documented for hydraulic hybrid heavy-duty vehicles are large, the regulatory landscape is shifting rapidly toward zero-tailpipe emissions, and battery-electric and hydrogen fuel-cell heavy-duty trucks are advancing in parallel. The hydraulic hybrid is therefore best understood not as a long-term replacement for these technologies but as a near-term, commodity-material solution for vocational duty cycles where its power density and durability are uniquely valuable, and as a potential complement to battery and fuel-cell traction in next-generation electro-hydraulic architectures.

10. Conclusions

The principal conclusions of this updated review may be summarized as follows.

(1) The series hydraulic hybrid architecture, particularly when augmented with a high-pressure air tank and a pressure exchanger as proposed in this work (Figure 14), offers theoretical regenerative-braking efficiencies in excess of 0.85 and real, component-loss-corrected efficiencies of 0.55-0.61 on pure stop-and-go duty cycles, falling to approximately 0.20-0.23 when a 40% cruise segment is added (Figure 21).

(2) Sub-system models of the diesel engine (Figure 15), bent-axis variable-displacement pump/motor (Figures 16-17), hydro-pneumatic accumulator, air tank with pressure exchanger and three-stage reciprocating compressor (Figures 18-19) have been integrated into a forward-facing closed-loop MATLAB/Simulink environment (Figure 13) that reproduces the qualitative behavior reported in the literature for the EPA/UPS Class IV demonstration vehicle and for the Eaton HLA refuse-truck program.

(3) Recent commercial and demonstration data, including the more than 100 in-service Eaton HLA refuse trucks, Parker Hannifin's RunWise series hybrid, the Lightning Hybrids parallel retrofit kit (Figure 22), and the 2024 real-driving emissions campaign on a Euro IV diesel truck, confirm that fuel-consumption reductions in the range 17-35% and brake-life extensions of four- to six-fold are routinely attainable on vocational duty cycles (Figure 24).

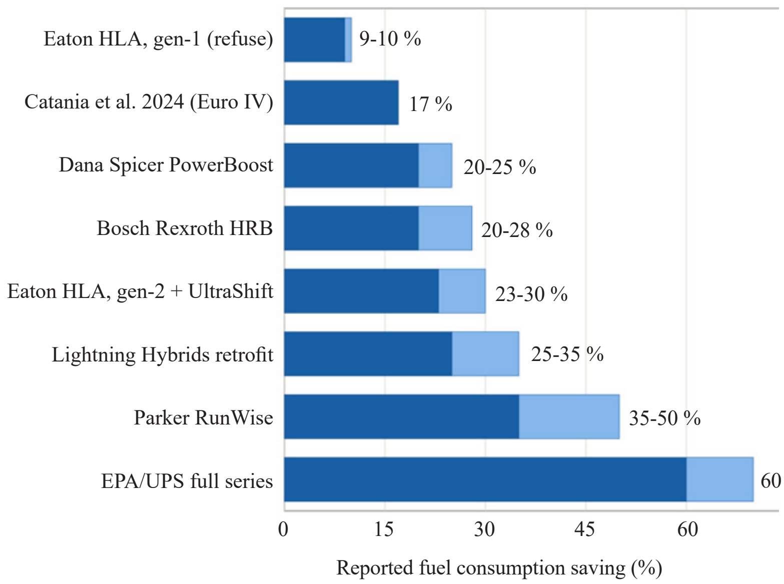

Figure 24. Reported fuel-consumption savings for commercial and demonstration hydraulic hybrid systems on representative urban or vocational duty cycles

(4) The Euro VII regulation (Regulation (EU) 2024/1257) and the revised heavy-duty-vehicle CO_2 standard (Regulation (EU) 2024/1610), which mandate fleet-average CO_2 reductions of 45% by 2030, 65% by 2035 and 90% by 2040 and a 100% zero-emission target for new urban buses by 2035, will progressively force the integration of hydraulic hybrid components with battery-electric or fuel-cell traction systems in electro-hydraulic hybrid architectures. The very high specific power and cycle durability of the hydro-pneumatic accumulator (a ratio of approximately 71 : 21 over electrochemical batteries on the regeneration of urban-cycle braking energy, Figure 1) make it an attractive complement to electrochemical storage in such configurations.

(5) Future work should focus on (i) supervisory power-management strategies combining model-based

optimization with online learning, (ii) integration of the hydro-pneumatic accumulator with battery-electric and fuel-cell traction systems, and (iii) plug-in pre-charging of the air tank or high-pressure accumulator at fleet depots.

Acknowledgments

The author expresses gratitude to the Automotive Engineering Department of Çukurova University in Adana. The simulation study was initiated while he was working at the Automotive Engineering Department of Çukurova University on hydraulic hybrid heavy duty vehicles.

Conflict of interest

The author declares no conflict of interest.

References

[1] European Automobile Manufacturers' Association (ACEA), "CO_2 standards for heavy-duty vehicles," Fact Sheet, ACEA, Brussels, Belgium, 2023.

[2] European Union, "Regulation (EU) 2024/1257 of the European Parliament and of the Council of 24 April 2024 on type-approval of motor vehicles and engines and of systems, components and separate technical units intended for such vehicles, with respect to their emissions and battery durability (Euro 7)," *Official Journal of the European Union*, L Series, May 8, 2024.

[3] European Union, "Regulation (EU) 2024/1610 amending Regulation (EU) 2019/1242 as regards strengthening the CO_2 emission performance standards for new heavy-duty vehicles and integrating reporting obligations," *Official Journal of the European Union*, L Series, Jun. 6, 2024.

[4] National Research Council, "Review of the 21st century truck partnership: second report," National Research Council, Washington, DC, USA, Tech. Rep. 13288, 2012.

[5] J. Wang, P. Liu, J. Hicks-Garner, E. Sherman, S. Soukiazian, M. Verbrugge, H. Tataria, J. Musser, and P. Finamore, "Cycle-life model for graphite-$LiFePO_4$ cells," *Journal of Power Sources*, vol. 196, no. 8, pp. 3942-3948, 2011.

[6] W. J. B. Midgley and D. Cebon, "Comparison of regenerative braking technologies for heavy goods vehicles in urban environments," *Proceedings of the Institution of Mechanical Engineers, Part D: Journal of Automobile Engineering*, vol. 226, no. 7, pp. 957-970, 2012.

[7] United States Environmental Protection Agency, "Hydraulic Hybrid Vehicles Demonstration Project," *EPA Office of Transportation and Air Quality, Ann Arbor, MI, USA*, 2006-2024. [Online]. Available: https://www.epa.gov/cati/hydraulic-hybrid-vehicles. [Accessed Apr. 30, 2026].

[8] J. Kargul, "Advanced hydraulic hybrids delivering real-world savings" in Proc. Green Truck Summit, Indianapolis, IN, USA, 2013.

[9] National Research Council, "Medium-and heavy-duty hybrid vehicles," ch. 4, in *Reducing the Fuel Consumption and Greenhouse Gas Emissions of Medium-and Heavy-Duty Vehicles, Phase Two: First Report*, Washington, DC, USA: The National Academies Press, 2014, pp. 59-77.

[10] M. I. Ramdan and K. A. Stelson, "Optimal design of a power-split hybrid hydraulic bus," *Proceedings of the Institution of Mechanical Engineers, Part D: Journal of Automobile Engineering*, vol. 230, no. 12, pp. 1699-1718, 2016.

[11] California Energy Commission, "Hydraulic Hybrid Vehicle Demonstration," California Energy Commission, Sacramento, CA, USA, Final Project Report CEC-600-2019-061, 2019.

[12] N. C. Surawski, M. Awadallah, E. Zhao, S. Zhou, T. Dunn, C. Hall, and P. D. Walker, "Reducing real driving fuel consumption and emissions with a hydraulic hybrid vehicle," *Science of the Total Environment*, vol. 954, pp. 176549, 2024.

[13] K.-E. Rydberg, "Energy efficient hydraulic hybrid drives," in Proc. 11th Scandinavian Int. Conf. on Fluid Power (SICFP), Linköping, Sweden, 2009.

[14] D. Assanis, Z. Filipi, S. Gravante, D. Grohnke, X. Gui, L. Louca, G. Rideout, J. Stein, and Y. Wang, "Validation

and use of SIMULINK integrated, high fidelity, engine-in-vehicle simulation of the International Class VI truck," SAE Tech. Paper 2000-01-0288, Warrendale, PA, USA, 2000.
[15] Y. J. Kim and Z. Filipi, "Simulation study of a series hydraulic hybrid propulsion system for a light truck," SAE Tech. Paper 2007-01-4151, Oct. 2007.
[16] A. Pourmovahed, N. H. Beachley, and F. J. Fronczak, "Modeling of a hydraulic energy regeneration system-Part I: Analytical treatment," *Journal of Dynamic Systems, Measurement and Control*, vol. 114, no. 1, pp. 155-159, 1992.
[17] P. Pichot, *Compressor Application Engineering, Volume 1: Compression Equipment*. Houston, TX, USA: Gulf Publishing, 1986.
[18] R. Joel, *Basic Engineering Thermodynamics*, 4th ed. Harlow, U.K.: Longman Scientific and Technical, 1987.
[19] M. D. Burghardt, *Engineering Thermodynamics with Applications*, 3rd ed. New York, NY, USA: Harper & Row, 1986.
[20] W. J. B. Midgley, H. Cathcart, and D. Cebon, "Modelling of hydraulic regenerative braking systems for heavy vehicles," *Proceedings of the Institution of Mechanical Engineers, Part D: Journal of Automobile Engineering*, vol. 227, no. 7, pp. 1072-1084, 2013.
[21] M. Lammert, "Hydraulic hybrid and conventional package delivery vehicles: measured laboratory fuel economy on targeted drive cycles," National Renewable Energy Laboratory, Golden, CO, USA, Tech. Rep. NREL/TP-5400-62408, SAE Tech. Paper 2014-01-2375, 2014.
[22] F. Wang, Q. Wen, and B. Xu, "An energy saving rule-based strategy for electric-hydraulic hybrid wheel loaders," *Proceedings of the Institution of Mechanical Engineers, Part D: Journal of Automobile Engineering*, vol. 238, no. 13, pp. 4081-4092, 2024
[23] H. Liu, "Summary of research on key technologies and energy management of electro-hydraulic hybrid powertrain," *Journal of Southwest Jiaotong University*, vol. 59, no. 3, pp. 600-614, 2024.
[24] B. Huang, W. Yu, M. Ma, X. Wei, and G. Wang, "Artificial-intelligence-based energy management strategies for hybrid electric vehicles: a comprehensive review," *Energies*, vol. 18, no. 14, pp. 3600, 2025.
[25] A. N. F. Abdelbaky, A. Babangida, A. B. Kunya, and P. T. Szemes, "Development and fuel economy optimization of series-parallel hybrid powertrain for van-style VW Crafter vehicle," *Energies*, vol. 18, no. 14, pp. 3688, 2025.
[26] E. M. Szumska, "Regenerative braking systems in electric vehicles: a comprehensive review of design, control strategies, and efficiency challenges," *Energies*, vol. 18, no. 10, pp. 2422, 2025.
[27] J. Cao and A. Emadi, "A new battery/ultracapacitor hybrid energy storage system for electric, hybrid, and plug-in hybrid electric vehicles," *IEEE Transactions on Power Electronics*, vol. 27, no. 1, pp. 122-132, 2012.
[28] L. Li, T. Zhang, L. Lu, K. Ma, and Z. Sun, "Energy conversion and management strategies for electro-hydraulic hybrid systems: a review," *Sustainability*, vol. 17, no. 22, pp. 10074, 2025.
[29] T. C. Do, T. Q. Dinh, Y. Yu, and K. K. Ahn, "Innovative powertrain and advanced energy management strategy for hybrid hydraulic excavators," *Energy*, vol. 282, pp. 128951, 2023.
[30] V. H. Nguyen, T. C. Do, T. D. Dang, and K. K. Ahn, "Improving the efficiency of hybrid hydraulic excavators with a novel powertrain and energy management system," *Energy*, vol. 323, pp. 135766, 2025.